Powder Technology 360 (2020) 104–111

Contents lists available at ScienceDirect

Powder Technology

journal homepage: www.elsevier.com/locate/powtec

Granular flow in a silo discharged with a conveyor belt

Diego Gella*, Diego Maza, Iker Zuriguel

Departamento de Física y Matemática Aplicada, Facultad de Ciencias, Universidad de Navarra, Pamplona, Spain

ARTICLE INFO

Article history:
Received 28 February 2019
Received in revised form
26 September 2019
Accepted 1 October 2019
Available online 10 October 2019

Keywords:
Silo
Flow
Conveyor belt
Granular matter

ABSTRACT

By means of an experimental analysis we study the granular flow in a two-dimensional silo discharged through a conveyor belt placed below the outlet. The results exhibit a saturation of the flow rate, W, with the belt velocity, v_b. Moreover, we find a dependence of the flow rate and grains velocity on the outlet size D which differs from the purely gravitational regime. To explain it, we propose an analysis based on mass conservation arguments that agrees with the experimental data when v_b is sufficiently low. For large values of this variable, it seems to be a smooth transition between a free discharge regime (for small D) and a belt extraction regime (for large D) where the proposed model is also valid. Our analysis provides a useful connection between the flow rate and the exit geometry, a feature that may be very useful from a practical point of view.

1. Introduction

In industry, both the extraction of raw materials and the goods production frequently result in the generation of granular matter. That is why there has been an unceasing motivation to study the specific features of this kind of materials for years [1]. The knowledge of their properties, unique and often counterintuitive, is of great importance to improve the efficiency of some industrial processes as manufacturing, transporting or storing. About the latter one, the study of the granular flow in silos is a topic under active research at present time [2–8]. However, the first works on this subject date back already from the eighteen century. In fact, in a paper from 1852 [9,10], Hagen observed the pressure saturation with the height of grains in silos (an idea that was lately developed by Janssen [11]) and found a flow rate dependence on the orifice size raised to the 5/2 power when the silos were discharged freely by gravity. This relationship, obtained from a dimensional analysis, was expressed a century later by Beverloo et al. [12] as:

$$W = C\rho_B\sqrt{g}(D - kd_p)^{5/2} \tag{1}$$

where ρ_B is the bulk density, g is the gravity acceleration, d_p is the particles size, $D = 2R$ is the orifice diameter, and C and k are fitting parameters. Remarkably, this k parameter introduces an empirical degree of freedom that was interpreted as a reduction of the silo effective aperture. The Hagen-Beverloo equation approximation resulted to be very useful, what is evidenced by its wide application to many scenarios [13–15], some of them beyond dry granular media [16,17]. Other expressions to predict the flow rate have been introduced more recently [18]. One of them comes from the experimental measurements of vertical velocity and solid fraction profiles at the outlet in a two-dimensional vertical silo. In Ref. [19], Janda et al. showed that those profiles were self-similar and proposed analytical expressions for the magnitudes from which they integrated an equation for the flow rate. According to this framework, which has been used afterwards by various authors [20–22], the profiles of vertical velocity $v_z(x)$ and solid fraction $\varphi^S(x)$ in the horizontal direction (x) can be written as:

$$v_z(x) = v_c\left(1 - (x/R)^2\right)^{1/\mu} \tag{2}$$

$$\varphi^S(x) = \varphi_c^S\left(1 - (x/R)^2\right)^{1/\nu} \tag{3}$$

where μ and ν are fitting parameters whereas v_c and φ_c are the values of $v_z(x)$ and $\varphi^S(x)$ at the center of the orifice ($x = 0$) respectively. Note that $\varphi^S(x)$ refers to the two-dimensional solid fraction of a monolayer of spheres, calculated as the projection of the 3D volume fraction (φ^V) on the xz plane. These quantities can be related to the mean values over the whole orifice by the integration of Eqs. (2) and (3), that is, $\langle v_z\rangle = \xi(\mu)v_c$ and $\langle\varphi^S\rangle = \xi(\nu)\varphi_c$, where $\xi(\chi) = \int_0^1 (1 - (x/R)^2)^{1/\chi}dx$ [21]. Furthermore, the dependence of v_c on the aperture size is described by means of:

* Corresponding author.
E-mail address: dgella@alumni.unav.es (D. Gella).

https://doi.org/10.1016/j.powtec.2019.10.030
0032-5910/

$$v_c(R) = \sqrt{2\gamma g R} \tag{4}$$

where γ is a fitting parameter. This equation, that also comes from the Hagen's dimensional analysis, was supported by the idea that there would exist a curved region above the orifice at which the grains start feeling the gravity from a non-accelerated state [10]. In spite of the inaccuracy of this concept, the scaling was confirmed in later works [23,24]. The solid fraction dependence on the outlet size is expressed in terms of φ_c^S through the expression:

$$\varphi_c^S(R) = \varphi_\infty^S\left(1 - \alpha_1 e^{-R/\alpha_2}\right) \tag{5}$$

where φ_∞^S is the asymptotic value to which φ_c^S tends for large D and α_1 and α_2 are fitting parameters. Finally, the expression for the mass flow rate was obtained by the integration of $W = \int_A \rho v_z(x)\varphi^V(x)dS$, where A is the exit area and ρ is the density of the material, resulting in the following relation:

$$W = \frac{2}{3}\int_A \rho\varphi^S(x)v_z(x)dS = C''\varphi_\infty^S\left[1 - \alpha_1 e^{-R/\alpha_2}\right]R^{3/2} \tag{6}$$

where C'' is a constant that depends on the previous fitting parameters: γ, ν and μ. The $2/3$ factor has been introduced to include the 3D volume fraction in Eq. (6), since in general $\varphi^V = \frac{2}{3}\varphi^S$. In addition, Eq. (6) recovers a $3/2$ power scaling, the exponent compatible with the Beverloo's fit for two-dimensional silos.

As we have seen, the silo discharged freely by gravity has captured the interest of scientists for years [25–27]. However, one of the most common ways to discharge silos in the industrial world is to extract the material with a conveyor belt placed below the orifice [28]. These devices allow the horizontal transport of raw materials in production lines, what became decisive in industrial process automatization due to substantial savings in staff costs.

Surprisingly, as far as we know, there has not been any work where the discharge rate is studied when the material is extracted with a conveyor belt. Indeed, there are only some investigations barely related to this topic, which can be grouped in two scenarios. In the first one the mechanical properties of the conveyor belt were studied when transporting granular materials [29,30]. In the second, other authors investigated the flow of grains on top of a conveyor belt passing through a bottleneck [31–34]. Chiefly, they found that the flow rate was proportional to the driving velocity when this was below a critical value. Above it, the flow rate saturated in a constant value that depended on the aperture size. It is worth noting that, from a physical point of view, this experiment and a vertical silo discharged through a conveyor belt are completely different. In the experiment about bottleneck flow of grains on a conveyor belt, the particles are dragged by the belt. Nevertheless, in the vertical silo, the gravity is the driving force and the conveyor belt, that runs perpendicularly respect to the grains outflow, is only responsible for braking the grains and moving them in the perpendicular direction. In that way, the combination between the gravity acceleration and the belt braking should determine the particles movement at the outlet.

Finally, we note that in a recent work of our group, a silo discharged by the action of a conveyor belt was experimentally studied but focusing mainly in the investigation of the clogging process due to arch formation [35]. This work pointed out the importance of using a conveyor belt as a method to control the grains velocity, suggesting the necessity of performing a detailed analysis of the discharge features in that setup.

2. Experimental setup

The experimental system used in this work, which is similar to the one used in Ref. [35], is depicted in Fig. 1 a). Essentially, two 0.6 cm thick transparent glass sheets of 61.2×160 cm^2 are set in parallel. Between them there are two 0.4 cm thick aluminum pieces at both lateral sides of the glasses. They are supplemented by thin strips of cardboard, in such a way that only a single layer of monodisperse stainless steel AISI 420 spheres of diameter $d_p = 0.4$ cm, fits inside. The aluminum pieces play the role of silo walls, and their thickness, that can be approached to $s = 0.4$ cm by neglecting the cardboard thickness, are also the extent of the silo in the y-direction. Additionally, there are two wedge-shaped stainless steel pieces at the silo bottom whose separation defines the outlet size $D = 2R$. Another parameter to take into account is the horizontal distance between the bottom part of both steel pieces, which is $D + 2\Delta$ with $\Delta = 0.5$ cm (see Fig. 1 c)). Furthermore, there is a hopper at the top of the silo through where the grains can be poured. The system is complemented with a conveyor belt made of honeycomb rubber that runs with a velocity v_b ranging from 0.1 to 16 cm/s. It was placed just below the orifice, at a distance of $h = 0.67 \pm 0.03$ cm measured between the bottom part of the silo and the upper protrusions of the honeycomb texture of the belt. This arrangement can be appreciated both in Fig. 1 b), which is a zoomed photograph of the outlet region taken from the rear of the silo, and in Fig. 1 c), a schematic view of the same area where some magnitudes are illustrated. In the former it can be seen that the grains fall on the belt, which brakes them and determines their collective movement. Therefore, this layout allows us to control the flow rate by means of the v_b.

The objective of this work is to investigate how the flow rate W and other related magnitudes depend on v_b and also on the outlet geometry. Those magnitudes can be obtained through the processing of videos taken at the region where the granular material flows out the silo. To record them we used a high speed camera *Photron Fastcam-1024 PCI 100K* placed in front of the outlet region, in combination with a LED panel at the rear to enhance the contrast of the images. We have acquired several videos with a frame rate between 250 and 1000 fps sweeping two variables: v_b and D. The subsequent particle tracking software is able to detect the beads position in each frame. From them, each bead is linked with its position in the next frame and the single velocities $\vec{v_i}$ are calculated as the quotient between the displacement and the time lapse between both frames. For calculating the flow rate, the software simply registers the number of particles that pass trough the outlet line ($z = 0$) at each frame.

In addition, the profiles of solid fraction and velocity are obtained from continuous maps computed with a coarse-graining tool developed in Refs. [36,37]. According to that technique, the magnitudes are calculated in the following way:

$$\varphi^S(\vec{r}, t) = A_p\sum_{i=1}^{N}\Theta(\vec{\mathscr{R}_i}(t)) \tag{7}$$

$$\vec{v}(\vec{r}, t) = A_p\sum_{i=1}^{N}\vec{v}_i\Theta(\vec{\mathscr{R}_i}(t)) \Big/ \varphi^S(\vec{r}, t) \tag{8}$$

where $\Theta(\vec{\mathscr{R}_i}(t))$ is a normalized coarse-graining function, N is the total number of particles in the frame, $A_p = \pi r_p^2$ is the particle's area and $\vec{\mathscr{R}_i}(t) = \vec{r} - \vec{r_i}(t)$, being $\vec{r_i}(t)$ the position vector of the particle i at time t. In order to avoid distorting the magnitudes near the boundaries we used a two-dimensional Heavyside step function with a characteristic length equal to the particle radius ($w = r_p$), that is

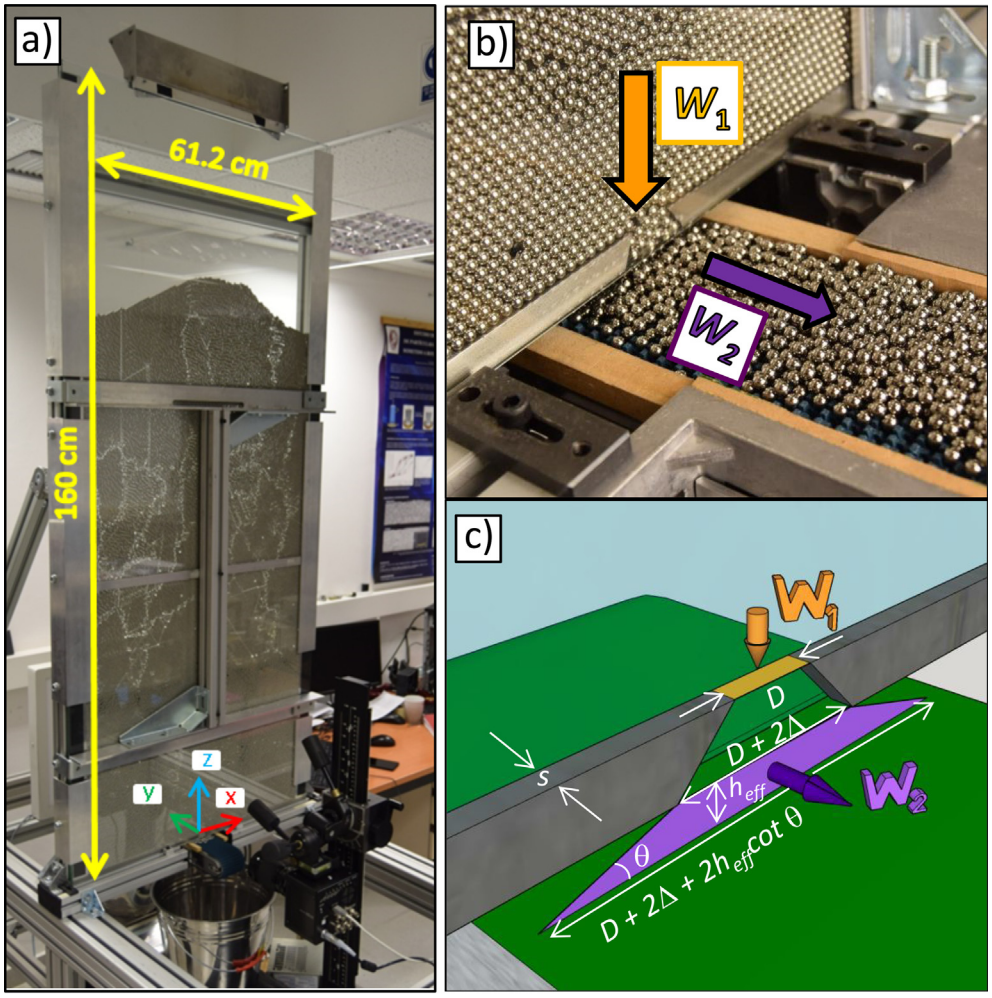

Fig. 1. a) General view of the experimental system. Note that the origin of the cartesian coordinates axes is placed at the center of the orifice size. b) Rear photograph of the outlet region of the experimental setup. c) Sketch of the same region where some magnitudes are defined. According to the model explained in the text, the orange rectangle represents the area through which the grains cross the outlet and the purple trapeze depicts the area through which the grains come out the silo. (For interpretation of the references to colour in this figure legend, the reader is referred to the Web version of this article.)

$$\Theta(\overrightarrow{\mathscr{R}_i}(t)) = \frac{1}{A_p} H(r_p - |\overrightarrow{\mathscr{R}_i}(t)|) \tag{9}$$

In other words, this coarse-graining tool assigns the velocity and density values to all the area covered by the particles and not only to their center. Finally, the profiles of both magnitudes at the outlet line are extracted as the values of the maps at $z = 0$ averaged over time.

3. Flow rate

In Fig. 2 a) the experimental outcomes of W are represented as function of v_b for five different outlet sizes. As expected, the curves show an increasing trend in all cases. However, for small D values, specially for the lowest one ($D = 1.61$ cm) the data tend to saturate in a constant value of W for high values of v_b. Thus, no matter how much the extraction velocity is raised, the flow rate will not grow anymore. This result resembles the saturation obtained in Refs. [31–34] for the experiment where disks dragged by a horizontal conveyor belt were made to pass through a bottleneck on top of it.

Aiming at understanding the nature of this dependence, in Fig. 2 b) we represent the same data than in Fig. 2 a), but plotting W as function of D. There we include the experimental results of W for the free discharge regime (that is, measured in an identical setup but without settling a belt below the outlet) reported in Ref. [20] as well as provide the analytical expression that reproduces them. This free discharge scenario clearly constitutes an upper limit for the flow rate because the belt only can brake the grains movement and they are never accelerated beyond the case without belt. Indeed, this is basically the reason for which the data saturate for high values of v_b in Fig. 2 a). Furthermore, from Fig. 2 b) we can state that given a certain belt velocity, the flow rate grows with D in a much less pronounced way than in the free discharge experiment.

4. Velocity and solid fraction profiles

In order to thoroughly analyze the mechanism behind the flow rate dependence on v_b and D reported in Fig. 2, we carried out a detailed study of the vertical velocity and packing fraction profiles just at the outlet line ($z = 0$). Fig. 3 a) shows the experimental v_z profiles as function of x (the horizontal coordinate) for different values of D and v_b. For each D we observe profiles with the same apparent shape but whose height grows with v_b. Moreover, comparing the curves with the same v_b, we observe that the maximum velocity do not seem to vary considerably with D. This behaviour contrast to the D-dependence of the curves corresponding to the free discharge case, whose magnitude visibly

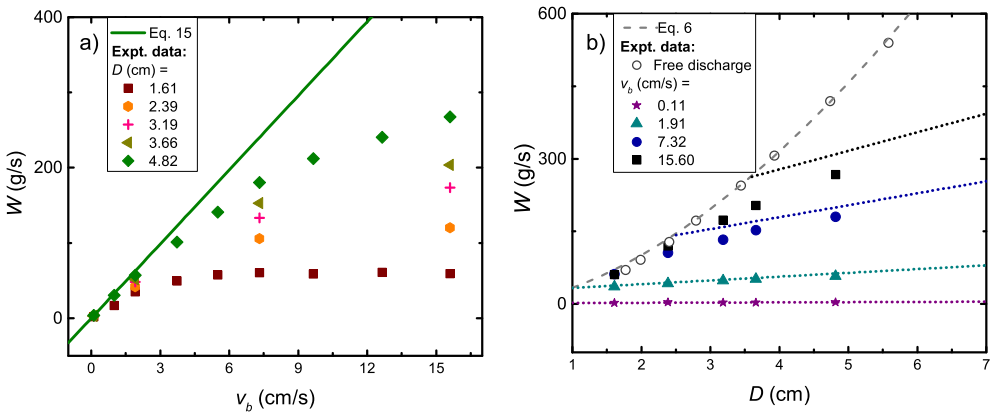

Fig. 2. a) Experimental data of W as function of the v_b for the orifice sizes displayed in the legend. The solid line is Eq. (15) for $D = 4.82$ cm and $K_\varphi = 1.06$ as explained in the text. b) Experimental data of W versus D for the free discharge case (empty circles, data taken from Ref. [20]) and for different belt velocities (full symbols) as shown in the legend. The dashed line corresponds to Eq. (6) and the dotted lines are representations of Eq. (15) for each v_b (with their corresponding K_φ as displayed in Table 2).

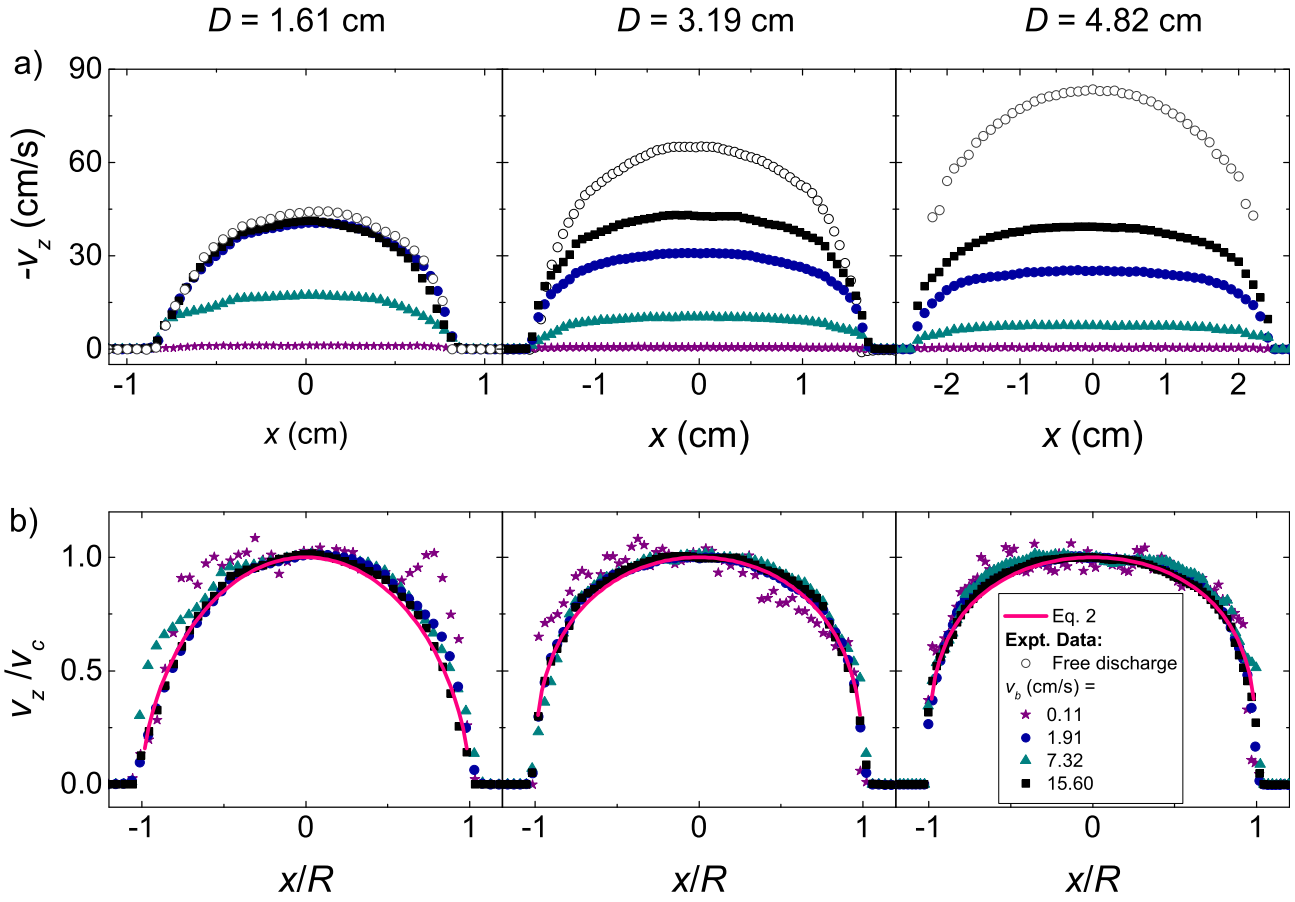

Fig. 3. a) Experimental profiles of v_z vs x for the free discharge scenario (empty circles, data taken from Ref. [20]) and for several values of v_b (full symbols) as shown in the legend. Different panels are used for distinct values of D. b) Collapse of the profiles obtained for the belt extraction procedure when v_z and x are rescaled by v_c and R respectively. The solid lines are fits of Eq. (2) with the parameters displayed in Table 1.

increases with D. The collapse of the data when v_z and x are rescaled by v_c and R respectively, are represented in Fig. 3 b). There, we note that the outcomes for $v_b = 0.11$ cm/s are quite noisy. The reason is probably a lack of statistics given that the belt velocity is so low that the beads cover very short distances over the typical film duration. Even so, it is remarkable that the curves collapse reasonably well and they all can be described by Eq. (2) with the same fitting parameter μ for each outlet size. From this we can conclude that: i) the functionalities of the velocity profiles obtained in a free discharged silo are still valid when the grains are extracted with a belt; ii) the fitting exponents do not depend on v_b but they do on D. The relation among the values of μ (and their corresponding $\xi(\mu)$ as defined in section 1) and D is presented in Table 1. The increasing trend of either μ and $\xi(\mu)$ with D reveals that the profiles become flatter as the outlet size increases.

Likewise, the profiles of φ^S vs x are represented in Fig. 4 a) for the same values of D and v_b. In this case, the curves show slightly wavy patterns indicating a certain degree of ordering in the spatial

Table 1
Exponent values (μ and ν) obtained from the fits of the velocity and density profiles with Eqs. (2) and (3), as function of D. Also, their corresponding $\xi(\mu)$ and $\xi(\nu)$ parameters are displayed.

$D(cm)$	μ	ν	ξ(μ)	ξ(ν)
1.61	1.9	3.6	0.769	0.862
2.39	2.4	7.0	0.812	0.922
3.19	2.9	7.8	0.837	0.929
3.66	2.9	8.3	0.837	0.933
4.82	3.4	8.4	0.934	0.934

corresponding constants described above (see Table 1). Looking first to Fig. 5 a), we observe that the values of $\langle v_z \rangle$ are in general much larger than their corresponding values of v_b. In addition, we find that, contrary to what could be expected, $\langle v_z \rangle$ slightly decreases with D. This trend is opposite to the one displayed in the free discharge case (empty symbols in Fig. 5 a)) where the velocity of the grains monotonically grows with D. Furthermore, we observe that the free discharge regime plays the role of an upper limit for the $\langle v_z \rangle$, i.e. the grains velocity at the center can not exceed Eq. (4).

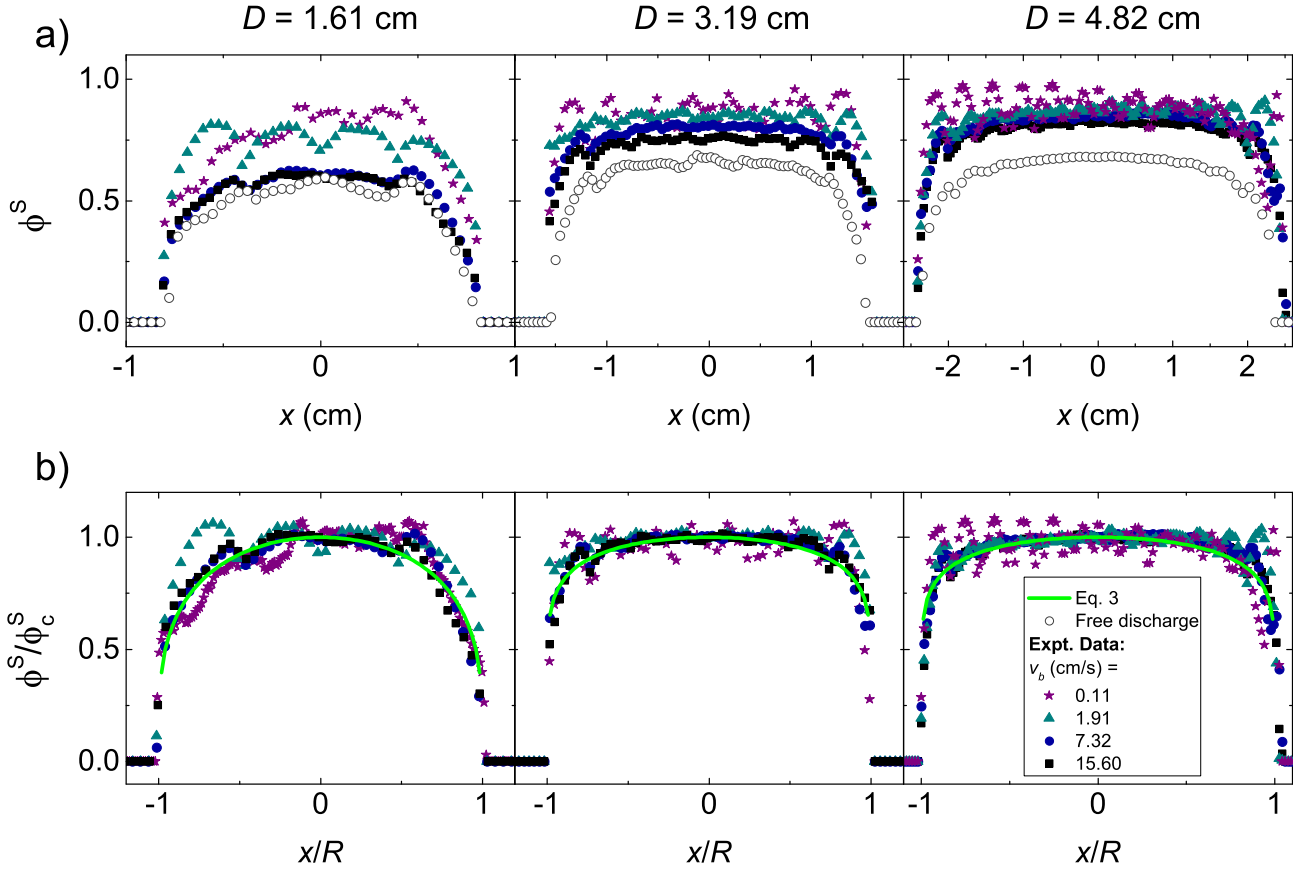

Fig. 4. a) Experimental profiles of φ^S vs x for the free discharge case (empty circles, data taken from Ref. [20]) and for several values of v_b (full symbols) as shown in the legend. Different panels are used for distinct values of D. b) Collapse of the profiles obtained for the belt extraction procedure when φ^S and x are rescaled by φ_c^S and R respectively. The solid lines are fits of Eq. (3) with the parameters displayed in Table 1.

configuration of the beads. Despite that, all density profiles have a similar general shape, although in this case the difference of trends between the free discharge regime and the rest is not as marked as in Fig. 3 a). Furthermore, the representation in Fig. 4 b) of the solid fraction profiles when φ^S and x are rescaled by φ_c^S and R respectively, suggests a similar behaviour than the one observed for the velocity profiles. Indeed, all profiles can be described by Eq. (3) with values of ν and $\xi(\nu)$ independent on v_b, but increasingly dependent on D (see Table 1); so the profiles flatten as the outlet size grows.

5. Velocity and solid fraction dependence on the outlet size

Now, in order to study in detail how the profiles evolve with the outlet size and the belt velocity, in Fig. 5 we have represented the values of $\langle v_z \rangle$ and $\langle \varphi^S \rangle$, as function of D (for different v_b values and for the free discharge case). For each D, these magnitudes have been calculated as $\langle v_z \rangle = \xi(\mu) v_c$ and $\langle \varphi^S \rangle = \xi(\nu) \varphi_c^S$ respectively, where v_c and φ_c^S are the values of v_z and φ^S at $x = 0$, and $\xi(\mu)$ and $\xi(\nu)$ are the

Regarding $\langle \varphi^S \rangle$, in Fig. 5 b) we see that all the curves show an increasing trend with D, appearing to saturate in an asymptotic value. Notably, the solid fractions for the belt extraction case seem to saturate in a higher value than the asymptotic value reached for the free discharge case, $\langle \varphi^S \rangle = \xi(\nu) \varphi_\infty^S$. In fact, the asymptotic value for the solid fractions reached with the belt seems to be near the closest packing fraction in 2D, $\varphi_{CP}^S = \frac{\pi\sqrt{3}}{6} \simeq 0.906$. This means that for this setup, given a certain v_b, there will always exist a sufficiently big orifice for which the material falls almost fully compacted.

6. Mass conservation analysis

In order to provide an analytical framework that encompasses all these results, we are going to perform an analysis based on mass conservation. When the grains flow out of the silo and settle on the belt, they form a pile whose section can be approximated by the violet area of Fig. 1 b). That region has a trapezoid shape, where θ is

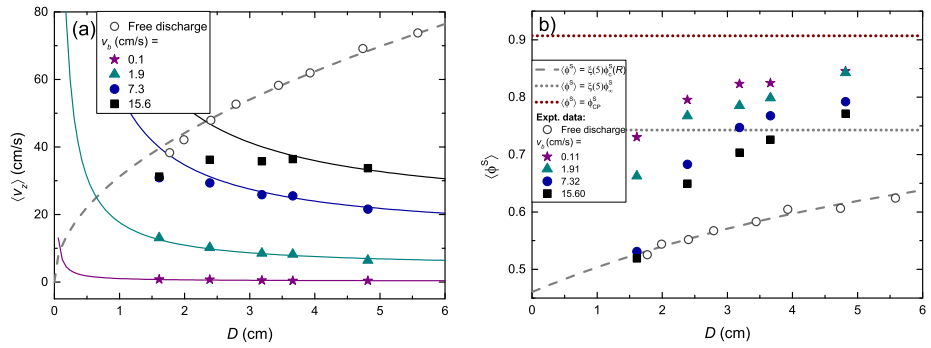

Fig. 5. a) Experimental data of $\langle v_z \rangle$ vs D for the free discharge case (empty circles, data taken from Ref. [20]) and for the values of v_b displayed in the legend (full symbols). The dashed line corresponds to Eq. $\langle v_z \rangle = \xi(\mu = 2.7)v_c(R)$, where $v_c(R)$ is given by Eq. (4), and the solid lines are the plots of Eq. (13) using the values of K_φ reported in Table 2 b) Experimental data of $\langle \varphi^S \rangle$ as function of D for the free discharge case (empty circles) and for the different values of v_b showed in the legend (full symbols). The dashed line corresponds to, where $\varphi_c^S(R)$ is given by Eq. (5), whereas the horizontal dotted lines are the limit values of $\langle \varphi^S \rangle$ for the free discharge case, $\langle \varphi^S \rangle = \xi(\nu = 5)\varphi_\infty^S$ (in brown) and for the extraction belt cases, $\langle \varphi \rangle = \varphi_{CP}^S$ (in gray) as explained in the text. (For interpretation of the references to colour in this figure legend, the reader is referred to the Web version of this article.)

the grains angle of repose and h_{eff} is the height of the pile, that may be slightly larger than h since some grains get into the hollows of the honeycomb texture of the belt. According to that, we can balance the mass flow rate that enters the orifice through the orange area and the mass flow rate that comes out the silo through the violet area (see Fig. 1 c)):

$$W = W_1 = W_2 \tag{10}$$

Assuming that the velocity v and the volume fraction φ^V are uncorrelated variables we can write:

$$W = \rho\langle\varphi_1^V\rangle\langle v_1\rangle A_1 = \rho\langle\varphi_2^V\rangle\langle v_2\rangle A_2 \tag{11}$$

where ρ is the material density. Moreover, we can consider that all grains are dragged in the perpendicular direction with the same velocity of the belt, so $\langle v_2 \rangle = v_b$ and then:

$$\langle v_1 \rangle = \frac{\langle\varphi_2^V\rangle}{\langle\varphi_1^V\rangle}\frac{A_2}{A_1}v_b \tag{12}$$

Thus, as a general case, the mean velocity at the outlet depends on the product of the quotient of areas, the quotient of volume fractions and the belt velocity. Considering our particular case, A_1 is the area of the outlet, $A_1 = sD$, and A_2 is the area of the violet trapeze in Fig. 1 c), $A_2 = (D + 2\Delta + h_{eff}\cot\theta)h_{eff}$. Naming the ratio of volume fractions as $K_\varphi = \frac{\langle\varphi_2^V\rangle}{\langle\varphi_1^V\rangle}$ we obtain an expression for $\langle v_1 \rangle$, which in our setup corresponds to $\langle v_z \rangle$:

$$\langle v_1 \rangle = \langle v_z \rangle = K_\varphi \frac{\left(D + 2\Delta + h_{eff}\cot\theta\right)}{sD} h_{eff} v_b \tag{13}$$

This equation shows a linear relationship with v_b and a dependence on the geometrical parameters (D, Δ, θ, h_{eff} and s), that comes from the quotient A_2/A_1. Remarkably, the inverse trend with D exhibited by Eq. (13) implies that, for a given v_b, $\langle v_z \rangle$ decreases when the outlet size grows (as it was shown in Fig. 5 a)). Looking at Eq. (13), it becomes patent the importance of K_φ, a variable that may depend on either v_b or D. In fact, it is logical to think that it does depend on v_b, specially in the limit of high values, when we are close to the gravitational regime. There, when v_b is increased, φ_2^V will necessarily decrease while φ_1^V will have a lower limit as it can not fall below the value reported for the free discharge. As a first approximation we will consider K_φ as independent on D, at least for sufficiently big outlet sizes far from the free discharge regime. Taking this into consideration, we plotted in Fig. 5 a) different expressions of Eq. (13). To do that, the repose angle and the effective height have been estimated in $\theta = 20^o$ and $h_{eff} = 0.75$ cm (slightly larger than h); therefore the only parameter we left free was K_φ for which we obtained the values displayed in Table 2. Remarkably, Eq. (13) is able to reproduce quite well the experimental data except for the small values of D and the greatest belt velocity studied ($v_b = 15.60$ cm/s), a scenario which is close to the free discharge region. Indeed, the experimental data can not follow Eq. (13) if the theoretical prediction leads to values above the free discharge scenario (Eq. (4)) as the material would have to move faster than if it would be accelerated by gravity, what is impossible in our system. Then, for small D and big v_b the grains stop feeling the belt and the system behaves as if discharged by gravity. Therefore, for each v_b, it seems that Eqs. (4) and (13) are the limits of v_c for low and high values of D respectively and there exists a smooth transition between both trends.

As we can see in Table 2, K_φ starts from 1.06 for the two lowest v_b and then gradually decreases as v_b grows. This suggests that as the belt velocity increases, the solid fraction in the region 2 (below the orifice) reduces as we speculated above. We see the limit value of 1.06 for very low v_b as the ratio between the volume fraction for a close-packed two-dimensional arrangement, $\varphi_{CP}^V = \frac{2}{3}\varphi_{CP}^S = \frac{\sqrt{3}}{9}\pi \simeq 0.604$ and for a random close packing of spheres, $\varphi_{RCP}^V = 0.64$. Thus, we considered that for the lowest v_b, the system passes from a fully packed 2D layer of grains to a random close packed 3D pile. In summary, from our mass conservation analysis we are able to obtain an excellent match of the experimental data for the lowest v_b by only using a fitting parameter, K_φ. Having said that, it should be noted that the choice of different values for h_{eff} or θ would lead to different values of K_φ as they are strongly interdependent.

Finally, we are going to use our mass conservation model to express the flow rate in terms of Eq. (13). From Eq. (11), $W = \rho\langle\varphi_2^V\rangle\langle v_2\rangle A_2$, using $\langle\varphi_2^V\rangle = K_\varphi\langle\varphi_1^V\rangle$ and substituting as before we obtain:

Table 2
Relationship of v_b and the values of K_φ used in the equations.

$v_b(cm/s)$	K_φ
0.11	1.06
1.91	1.06
7.92	0.85
15.60	0.62

$$W = \langle \varphi_1^V \rangle K_\varphi \rho \left(D + 2\Delta + h_{eff} \cot\theta \right) h_{eff} v_b \quad (14)$$

Given that we are evaluating the flow rate in the limit of large D and that there is an increasing trend of $\langle \varphi^S \rangle$, approaching φ_{CP}^S, we can make use of the approximation $\langle \varphi_1^V \rangle \approx \varphi_{CP}^V = \frac{\pi\sqrt{3}}{9} \simeq 0.604$ in that limit. Hence the mass flow rate can be described as:

$$W = \varphi_{CP}^V K_\varphi \rho \left(D + 2\Delta + h_{eff} \cot\theta \right) h_{eff} v_b \quad (15)$$

Using the values of K_φ shown in Table 2, we plotted Eq. (15) in Fig. 2 b) with solid lines. The outcomes resemble the ones observed for the velocities' graph. For low values of v_b, the agreement is good. For high v_b, however, the data follow the free discharge trend (Eq. (6)) for low D, and smoothly tend to an asymptotic behaviour (governed by Eq. (15)) as D grows. Note that for high values of v_b, the outcomes of W obtained for the range of D explored, are still far from the asymptotic behaviour. This is due to the fact that for such high values of v_b the corresponding values of φ^S are also far from φ_{CP}^S (see Fig. 5 b)). Thus, Eqs. (6) and (15) can be understood as the expressions governing the limit behaviour for low and high D respectively.

Regarding the expression of Eq. (15), we observe that the mass flow rate is linear with v_b. However, in Fig. 2 a) we observed that the flow rate saturated with that variable, so the indirect influence that v_b has on the flow rate through K_φ in Eq. (15) (see Table 2) should explain that behaviour. Indeed, in Fig. 2 we included the analytical expression proposed in this work (Eq. (15)) for $D = 4.82$ cm and the value of K_φ that corresponds to the lowest v_b (1.06). There we see how the experimental data obtained for that D (green diamonds) only follow the linear trend for the lowest values of v_b. For higher extraction velocities the values of W start curving downwards due to the decreasing v_b-dependence of K_φ. In fact, as the data tend to saturate in a constant value, Eq. (15) suggests that K_φ must be proportional to $1/v_b$ in the limit of high v_b. Furthermore, it should be noted that Eq. (15) is linear with D with an y-intercept different from zero. Therefore, in this equation the geometry plays a significant role since this y-intercept comes from A_2. Surprisingly, Eq. (15) also implies that (for very low values of v_b) the flow rate would be independent on the bottleneck section A_1 if it were possible to change A_2 without modifying A_1 (what is not the case of our setup since both areas depend on the control parameter D).

7. Effect of h_{eff}, the effective distance between the silo bottom and the belt

Up to now, all the results presented in this article make reference to experiments carried out with a system where the distance between the belt and the orifice is $h = 0.67 \pm 0.03$ cm. However, the magnitude of this parameter can play a crucial role in the description of the flow rate in this system. Indeed, the expressions 13 and 15 reveal a quadratic dependence of both the flow rate and the grains velocity on the effective distance h_{eff}, which comes from the computation of the trapezoidal cross-section A_2 of the pile of grains deposited on the belt. In order to test the validity of this approach, we performed new experiments for two additional values of $h = 0.32 \pm 0.03$ cm and $h = 0.46 \pm 0.03$ cm.

For these positions of the belt, we obtained the flow rate for $D = 1.61$ cm and two relatively slow belt velocities, $v_b = 1.91$ and 3.73 cm/s (recall that the scenario of low v_b values is where the application of the model works better). These experimental data are represented as function of h_{eff} (estimated in the same way than before, that is, $h_{eff} = h + 0.15$ cm) in Fig. 6. In this graph, the clear increasing trend indicates a noticeable effect of h_{eff} in the flow rate. Furthermore, the experimental flow rate is well described by Eq. (15) with values of $K_\varphi = 1.06$ for $v_b = 1.91$ cm/s and $K_\varphi = 0.89$ for $v_b = 3.73$ cm/s. This indicates that the mass conservation model proposed also recovers the influence of this parameter.

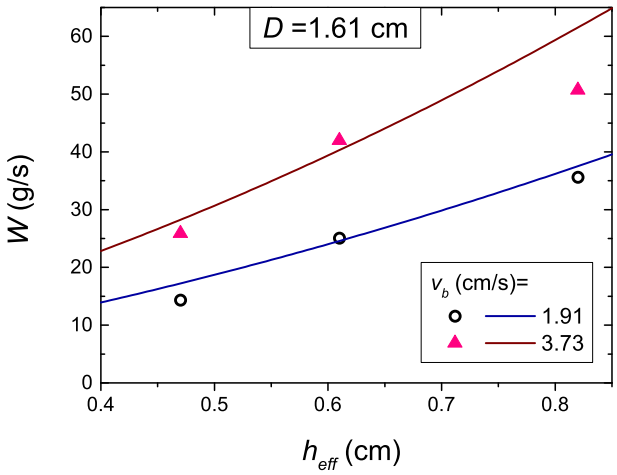

Fig. 6. Experimental flow rate as function of h_{eff}, the effective distance between the silo bottom and the conveyor belt, for $D = 1.61$ cm/s and the belt velocities indicated in the legend. The solid lines are plots of Eq. (15) with $K_\varphi = 1.06$ for $v_b = 1.91$ cm/s and $K_\varphi = 0.89$ for $v_b = 3.73$ cm/s.

8. Conclusions

We experimentally investigated the flow characteristics of granular material extracted from a two-dimensional silo using a conveyor belt. The outcomes showed a saturation of the flow rate with the velocity of the belt and a dependence of the flow rate on the orifice size considerably different to the free discharge case. In order to explain these observations we measured the solid fraction and velocity profiles at the outlet for several values of the belt velocity and the outlet size. Both resulted to be self-similar for every value of v_b and flatten as D increases, what allowed us to describe the profiles by using similar equations than for the free discharge case (Eqs. (2) and (3)). After the measurement of the dependence of these magnitudes at the center on D and making some approximations, we developed an analysis based on mass conservation. That framework is able to reproduce the behaviour of W and v_z vs D for low values of v_b, that is, when the conditions are far from the free discharge scenario.

Thus, the system displays a smooth transition from a free discharge regime governed by Eqs. (4)–(6) (for low D and high v_b, where the belt effect is not important), to the belt extraction regime (for high D and low v_b , Eqs. (13) and (15)). In the latter case, note that both, the nonlinearity in Eq. (13), and the non-zero y-intercept in Eq. (15), come from the relation between A_2 and A_1. This fact is very interesting from a practical point of view since it reflects the possibility of regulating the flow rate dependence on the extraction velocity by playing with the geometry of the exit. In particular, the effective distance h_{eff} is determinant in our setup due to its quadratic influence in both W and $\langle v_z \rangle$ (Eqs. (13) and (15)).

Even though, it should be noted that our setup is a particular experiment with certain geometrical and dynamic characteristics. However, the proposed analysis should be of general application and could be implemented in other systems with different configurations. In each case, the flow rate and outlet velocity will be determined from the computation of Eqs. (11) and (12), which involve several parameters that must be calculated or approached. By means of this procedure, it will be possible to predict the flow rate in systems with different geometrical configurations like silos including inclined or troughed belts, two widely used geometries that obviously affect the value of the area A_2 considered in Eqs. (11)

and (12). Also, an interesting research line could be the study of the effect of dynamical aspects like the friction between the particles and the belt, which will clearly affect the value of A_2 (through the angle of repose θ) and therefore be more important in the flow rate determination than, for example, the grains friction against the silo walls. Definitely, the applicability of the model proposed in this work can be tested in future works by means of its implementation to different experimental systems.

Acknowledgement

This work was funded by Ministerio de Economía y Competitividad (Spain) through Projects No. FIS2014-57325 and No. FIS2017-84631 MINECO/AEI/FEDER, UE Project.

References

[1] J. Duran, A. Reisinger, P.G. de Gennes, Sands, Powders and Grains: an Introduction to the Physics of Granular Materials. Partial Ordered Systems, Springer, New York, 2012.
[2] Y. Wang, Y. Lu, J.Y. Ooi, A numerical study of wall pressure and granular flow in a flat-bottomed silo, Powder Technol. 282 (2015) 43–54.
[3] P. Wang, L. Zhu, X. Zhu, Flow pattern and normal pressure distribution in flat bottom silo discharged using wall outlet, Powder Technol. 295 (2016) 104–114.
[4] H. Katsuragi, K.A. Reddy, K. Endo, Shape dependence of resistance force exerted on an obstacle placed in a gravity driven granular silo flow, AIChe Jounal 64 (2018) 3849–3856.
[5] K. To, H.-T. Tai, Flow and clog in a silo with an oscillating exit, Phys. Rev. E 96 (2017), 032906.
[6] J.P. Peralta, M.A. Aguirre, J.-C. Géminard, L.A. Pugnaloni, Apparent mass during silo discharge: nonlinear effects related to filling protocols, Powder Technol. 331 (2017) 265–272.
[7] A. Ashour, T. Trittel, T. Börszönyi, R. Stannarius, Silo outflow of soft frictionless spheres, Phys. Rev. Fluids 2 (2017) 123302.
[8] C. González-Montellano, A. Ramírez, E. Gallego, F. Ayuga, Validation and experimental calibration of 3D discrete element models for the simulation of the discharge flow in silos, Chem. Eng. Sci. 66 (2011) 5116–5126.
[9] G.H.L. Hagen, Aber den Druck und die Bewegung des trocknen Sandes, Bericht uber die zur Bekanntmachung geeigneten Verhandlungen der Koniglich Preussischen Akademie der Wissenschaften zu Berlin 35 (1852) 35–42.
[10] B.P. Tighe, M. Sperl, Pressure and motion of dry sand: translation of Hagen's paper from 1852, Granul. Matter 9 (2007) 141–144.
[11] H.A. Janssen, Versuche uber getreidedruck in silozellen, Z. Ver. Dtsch. Ing. 39 (1895) 1045–1049.
[12] W.A. Beverloo, H.A. Leninger, J. van de Velde, The flow of granular solids through orifices, Chem. Eng. Sci. 15 (1961) 260–269.
[13] H. Pacheco-Martínez, H.J. van Gerner, J.C. Ruiz-Suárez, Storage and discharge of a granular fluid, Phys. Rev. E 77 (2008), 021303.
[14] P. Arteaga, U. Tüzün, Flow of binary mixtures of equal-density granules in hoppers - size segregation, flowing density and discharge rates, Chem. Eng. Sci. 45 (1990) 205.
[15] S. Humby, U. Tüzün, A.B. Yu, Prediction of hopper discharge rates of binary granular mixtures, Chem. Eng. Sci. 53 (1998) 483.
[16] J. Koivisto, D.J. Durian, The sands of time run faster near the end, Nat. Commun. 8 (2017) 15551.
[17] Y. Bertho, C. Becco, N. Vandevalle, Dense bubble flow in a silo: an unusual flow of a dispersed medium, Phys. Rev. E 73 (2006), 056309.
[18] C. Mankoc, A. Janda, R. Arévalo, J.M. Pastor, I. Zuriguel, A. Garcimartín, The flow rate of granular materials through an orifice, Granul. Matter 9 (2007) 404–414.
[19] A. Janda, I. Zuriguel, D. Maza, Flow rate of particles through apertures obtained from self-similar density and velocity profiles, Phys. Rev. Lett. 108 (2012) 248001.
[20] D. Gella, D. Maza, I. Zuriguel, Role of particle size in the kinematic properties of silo flow, Phys. Rev. E 95 (2017), 052904.
[21] Y. Zhou, P. Ruyer, P. Aussillous, Discharge flow of a bidisperse granular media from a silo: discrete particle simulations, Phys. Rev. E 92 (2015), 062204.
[22] M. Madrid, K. Asencio, D. Maza, Silo discharge of binary granular mixtures, Phys. Rev. E 96 (2017), 022904.
[23] S. Dorbolo, L. Maquet, M. Brandenbourger, F. Ludewig, G. Lumay, H. Caps, N. Vandewalle, S. Rondia, M. Mélard, J. van Loon, A. Dowson, S. Vincent-Bonnieu, Influence of the gravity on the discharge of a silo, Granul. Matter 15 (2013) 263–273.
[24] S.M. Rubio-Largo, A. Janda, D. Maza, I. Zuriguel, R.C. Hidalgo, Disentangling the free-fall arch paradox in silo discharge, Phys. Rev. Lett. 114 (2015), 238002.
[25] R.M. Nedderman, U. Tüzün, S.B. Savage, G.T. Houlsby, The flow of granular materials–I: discharge rates from hoppers, Chem. Eng. Sci. 37 (1982) 1597–1609.
[26] S.B. Savage, Gravity flow of a cohesionless bulk solid in a converging conical channel, Int. J. Mech. Sci. 9 (1967) 651–659.
[27] P. Mort, J.N. Michaels, R.P. Behringer, C.S. Campbell, Kondic Lou, M. Kheiripour Langroudi, M. Shattuck, J. Tang, G.I. Tardos, C. Wassgren, Dense granular flow–A collaborative study, International Powder Technol 284 (2015) 571–584.
[28] C.R. Woodcock, J.S. Masdon, Bulk Solids Handling: an Introduction to the Practice and Technology, Springer Netherlands, 1988.
[29] G. Fedorko, V. Molnár, J. Zivcák, M. Dovica, N. Husáková, Failure Analysis of Textile Rubber Conveyor Belt Damaged by Dynamic Wear Engineering Failure Analysis, vol. 28, 2013, pp. 103–114.
[30] V. Molnár, G. Fedorko, B. Stehlíková, M. Tomasková, Z. Hulínová, Analysis of asymmetrical effect of tension forces in conveyor belt on the idler roll contact forces in the idler housing, Measurement 52 (2014) 22–32.
[31] B. De-Song, Z. Xun-Sheng, X. Guang-Lei, P. Zheng-Quan, T. Xiao-Wei, L. Kun-Quan, Critical phenomenon of granular flow on a conveyor belt, Phys. Rev. E 67 (2003), 062301.
[32] M.A. Aguirre, J.G. Grande, A. Calvo, L.A. Pugnaloni, J.C. Géminard, Pressure independence of granular flow through an aperture, Phys. Rev. Lett. 104 (2010) 238002.
[33] M.A. Aguirre, J.G. Grande, A. Calvo, L.A. Pugnaloni, J.C. Géminard, Granular flow through an aperture: pressure and flow rate are independent, Phys. Rev. E 83 (2011), 061305.
[34] M.J. Cordero, L.A. Pugnaloni, Dynamic transition in conveyor belt driven granular flow, Powder Technol. 272 (2015) 290–294.
[35] D. Gella, I. Zuriguel, D. Maza, Decoupling geometrical and kinematic contributions to the silo clogging process, Phys. Rev. Lett. 121 (2018) 138001.
[36] I. Goldhirsch, Stress, stress asymmetry and couple stress: from discrete particles to continuous fields, Granul. Matter 12 (2010) 239–252.
[37] T. Weinhart, C. Labra, S. Luding, J.Y. Ooi, Influence of coarse-graining parameters on the analysis of DEM simulations of silo flow, Granul. Matter 293 (2010) 138–148.